Ceramics International 47 (2021) 13837–13844

Contents lists available at ScienceDirect

Ceramics International

journal homepage: www.elsevier.com/locate/ceramint

High temperature interaction between Si–B alloys and Si_3N_4

Jian Meng Jiao [a,*], Kai Tang [b], Jafar Safarian [a], Bettina Grorud [a], Kathrine Sellevoll [a], Merete Tangstad [a]

[a] Norwegian University of Science and Technology (NTNU), Department of Materials Science and Engineering, N-7491, Trondheim, Norway
[b] SINTEF Materials and Chemistry, N-7491, Trondheim, Norway

ARTICLE INFO

Keywords:
Si–B alloys
Phase change material
Wettability
Si_3N_4
Thermal energy storage

ABSTRACT

Si_3N_4 is a candidate crucible material for Si–B alloys in high temperature thermal energy storage system. In this regard, the phase formation in the Si–B alloys and the interaction between the alloys and Si_3N_4 were investigated in an induction furnace at 1750 °C with the B addition of 2, 5, 8, and 11 mass %, respectively. Moreover, the wettability property of the Si-3.25B alloy (mass %) on Si_3N_4 substrate was examined at temperatures up to 1400 °C. The cross-sectional images and micro-analyses showed that BN precipitates were produced in the Si–B alloys and a BN layer was formed at the interface between the Si–B alloys and Si_3N_4. However, the amount of BN precipitates was negligible. Next, the equilibrium contact angle of liquid Si-3.25B alloy on Si_3N_4 substrate was determined to be 134 ± 1°, which indicates non-wetting behavior. The above results support that Si_3N_4 is a desirable refractory material for the high temperature thermal energy storage system.

1. Introduction

Latent heat thermal energy storage (LHTES) is one of the most efficient ways of storing thermal energy. Phase change materials (PCMs) offer state-of-the-art thermal energy storage due to high latent heat. Typically, PCM goes through a solid-liquid transformation to store energy in the form of latent heat. Si–B alloys are proposed as PCMs due to the fact that Si (1230 kWh/m^3) and B (2680 kWh/m^3) are the elements of the highest latent heat of fusion compared to other metals and salt hydrates [1].

The phase diagram of Si–B system has been widely investigated and is shown in Fig. 1. Three intermediate phases are formed in the system, SiB_3, SiB_6, and SiB_n. SiB_3 is stable at temperatures lower than 1270 °C, where it is in equilibrium with Si at B content lower than 58.7 mass % [2]. Increasing the temperature above 1270 °C, SiB_3 will be transformed to SiB_6 and Si, due to the reaction $2SiB_3 \rightarrow Si + SiB_6$. Moreover, a eutectic response occurs at 1385 °C, $Si + SiB_6 \rightarrow$ liquid, and hence above 1385 °C, SiB_6 is in equilibrium with liquid Si–B alloys. SiB_n is formed in the B rich part with a peritectic reaction at 2020 °C, Liquid + $B \rightarrow SiB_n$. In the application of Si–B alloys in the thermal energy storage system, Si–B alloys store and release energy by phase changes between solid phases and a liquid phase. It starts to melt at 1385 °C by absorbing a large amount of energy in the form of latent heat. However, the complete melting temperature depends on the B content, which decreases with the increase of B content in the B range of 0–3.25 mass %. Otherwise, it is increased with the increase of B content at B content higher than 3.25 mass % (eutectic point).

In order to apply the Si–B alloys to the thermal energy storage system successfully, the selection of proper refractory material is important to build the PCM container. Suitable refractory material should meet several requirements. It must be used at a higher temperature, as the lowest liquidus temperature of Si–B alloy is 1385 °C at the eutectic point. It should have the ability to defend against the liquid Si–B alloys corrosion after long-term thermal cycles. Moreover, it should not pollute the Si–B alloys. It has previously been observed that Si has high reactivity with refractory materials, which may result in severe damage to the container [3]. Therefore, the selection of the proper container is a challenge.

Three different refractory materials have been proposed: graphite, hexagonal BN (h-BN), and Si_3N_4. The interaction between Si–B alloys and graphite had been investigated at temperatures up to 1750 °C by the present author [4]. It has been found that a SiC layer was produced between graphite and Si–B alloys at B content lower than 3.25 mass %, while SiC and B_4C layers were formed between graphite and Si–B alloys at B content higher than 5 mass %. The formed layers can be used as a protective layer to prevent the penetration of liquid Si–B alloys to graphite. However, the formation of B_4C layer consumed some B in the Si–B alloys. It actually decreases the energy storage capacity of the Si–B

* Corresponding author.
E-mail address: jian.m.jiao@ntnu.no (J.M. Jiao).

https://doi.org/10.1016/j.ceramint.2021.01.249
Received 13 November 2020; Received in revised form 19 January 2021; Accepted 26 January 2021
Available online 30 January 2021

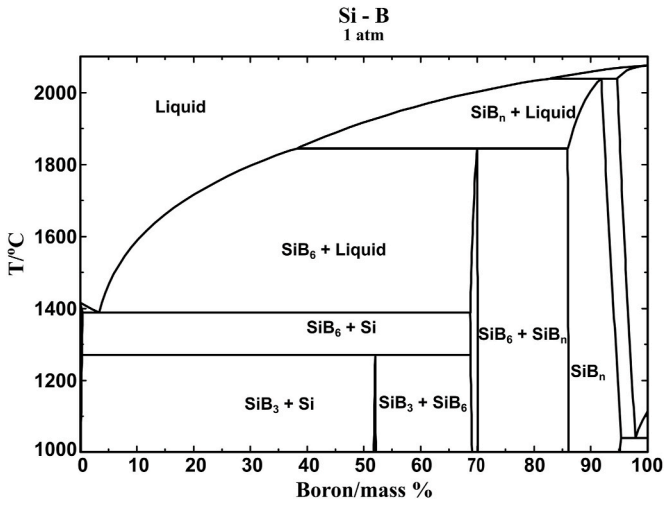

Fig. 1. Si–B binary phase diagram, calculated using the commercial FTlite database [3].

alloys. Furthermore, C solubility increased with the increase of B content in the liquid Si–B alloys, which would change Si–B alloys to Si–B–C (saturated) alloys.

h-BN is another refractory material to be used as Si–B alloys container. Polkowski et al. [5] investigated the wetting behavior of h-BN by liquid Si upon the melting/solidification process. The Si/h-BN was introduced to a sessile drop furnace subjected to 15 thermal cycles in the temperature range 1300–1450 °C under static Ar. It was observed that the contact angle was higher than 90° for the whole process. Moreover, the wetting behavior of the Si–B alloys on the h-BN substrate was investigated in the B range of 1–5.7 mass %, and the equilibrium contact angle was in the range 131–152° [6]. h-BN showed non-wetting with liquid Si–B alloys. However, it is better to operate the Si–B/h-BN system in an N_2 atmosphere, as the partial equilibrium pressure of N_2 is high at high temperatures [7].

Si_3N_4 is also suggested to be a potential Si–B alloys container at high temperatures. The existing body of research on Si_3N_4 indicates that it is often used in the production of Si for solar cells. Data from several studies show that the solubility of N in molten Si is in the range of 4–99.7 ppm mass at the temperature close to the melting point of Si [8–13]. Hence N as the introduced impurity is negligible in the Si. On the other hand, an oxynitride (Si_2N_2O) was formed at the interface of Si_3N_4 crucible after a few minutes of exposure to air at room temperature [14], which determined the wetting and infiltration properties of Si on Si_3N_4. Another significant aspect is that the mold coated with a layer of Si_3N_4 powder showed non-adhesion behavior with the solidified Si ingot [15]. Due to the promising properties of Si_3N_4, it is in this paper proposed as Si–B alloys container. The phase formation in the Si–B alloys, wettability property, and chemical interactions between Si–B alloys and Si_3N_4 were investigated experimentally and phase equilibrium calculations were used to establish reliable data on thermophysical properties of Si–B alloys in both solid and liquid states in the phase change process.

2. Experimental procedure and materials

The interaction of Si–B alloys with Si_3N_4 crucibles was first evaluated using an induction furnace, where 2, 5, 8, and 11 mass % of B powder (99.9%, Aladdin industrial company, China) were mixed with Si powder (SG-Si, United States), respectively. The Si_3N_4 crucible (Steuler solar GmbH, Norway) containing Si–B alloy was placed inside a big graphite crucible (IG-15, Svenska Tanso AB, Sweden). The Si_3N_4 was a conical shaped crucible, with 34 mm height, 4 mm wall thickness, 26 mm diameter at the top, and 22 mm diameter at the bottom. The height, wall thickness, and diameter of the graphite crucible were 150 mm, 7.5 mm, and 85 mm, respectively. 6 g Si–B alloy was placed in the Si_3N_4 crucible for each experiment. The graphite crucible was then located in the induction furnace and was thermally insulated by graphite felt. The temperature was measured at the inner bottom of the graphite crucible by the type-C thermocouple. The experiments were carried out at a temperature of 1750 °C for 2 h under an Ar atmosphere. Finally, the samples

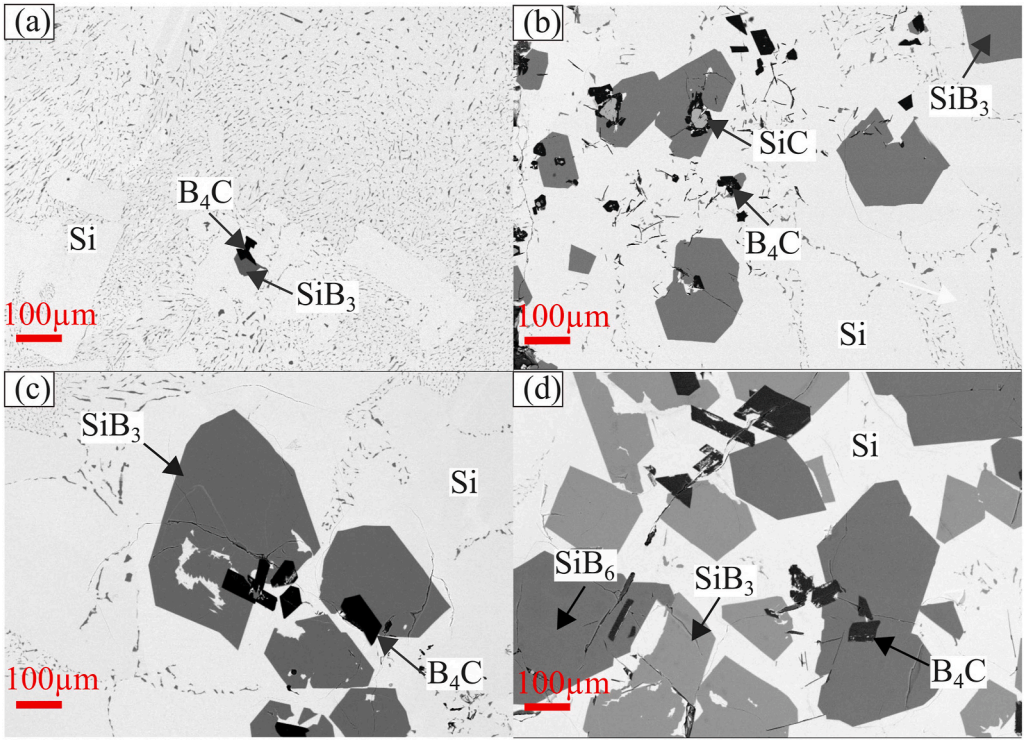

Fig. 2. BSE Images of the center part of the Si–B alloys after solidification. (a) 2 mass % B; (b) 5 mass % B; (c) 8 mass % B; (d) 11 mass % B.

Table 1
Chemical composition of the detected phases in the Si–B alloys, analyzed by SEM-EDS. (at. %).

	Si	B	N	C
BN	3.3	57.0	39.7	–
Si(ss)	98.9	0.4	–	0.7
SiB_3	28.9	71.1	0.01	–
SiB_6	15.4	84.6	–	–
B_4C	1.8	79.2	0.6	18.4
SiC	48.4	–	–	51.6

were cooled with the furnace.

The wettability of Si-3.25B alloy (3.25 mass % B) on Si_3N_4 substrate was determined in a sessile drop furnace. The Si_3N_4 substrate was cut to a plate with a diameter of 10 mm and a height of 3 mm. The Si-3.25B piece was first produced in a graphite crucible at 1750 °C under an Ar atmosphere, where the B content was confirmed to be 3.21 mass % [4]. Then it was placed on the Si_3N_4 substrate. Heating was performed in a vacuum of 10^{-4} atm to 1100 °C in 4 min, and then a gradual increase in the temperature up to 1350 °C with a heating rate of 20 °C/min. As the theoretical melting point of Si-3.25B alloy was 1385 °C, the heating rate was decreased to 5 °C/min to observe the melting process in the

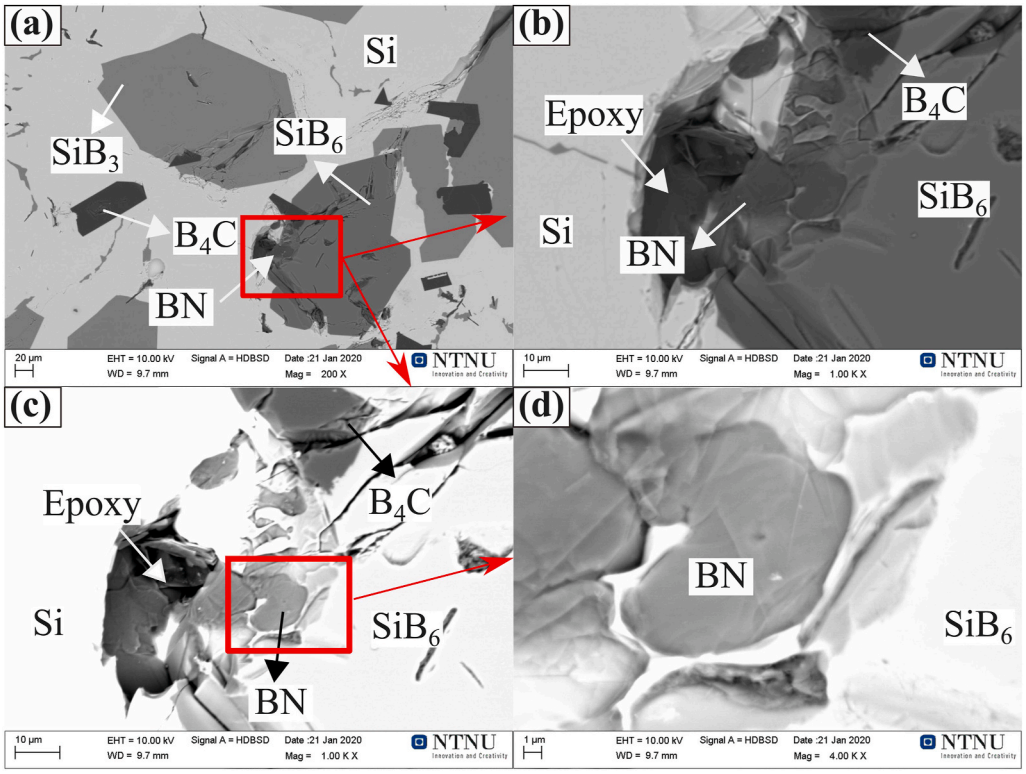

Fig. 3. BSE Images of the Si–8B alloy after solidification. (a) 200X; (b) low contrast at 1000X; (c) high contrast at 1000X; (d) 4000X

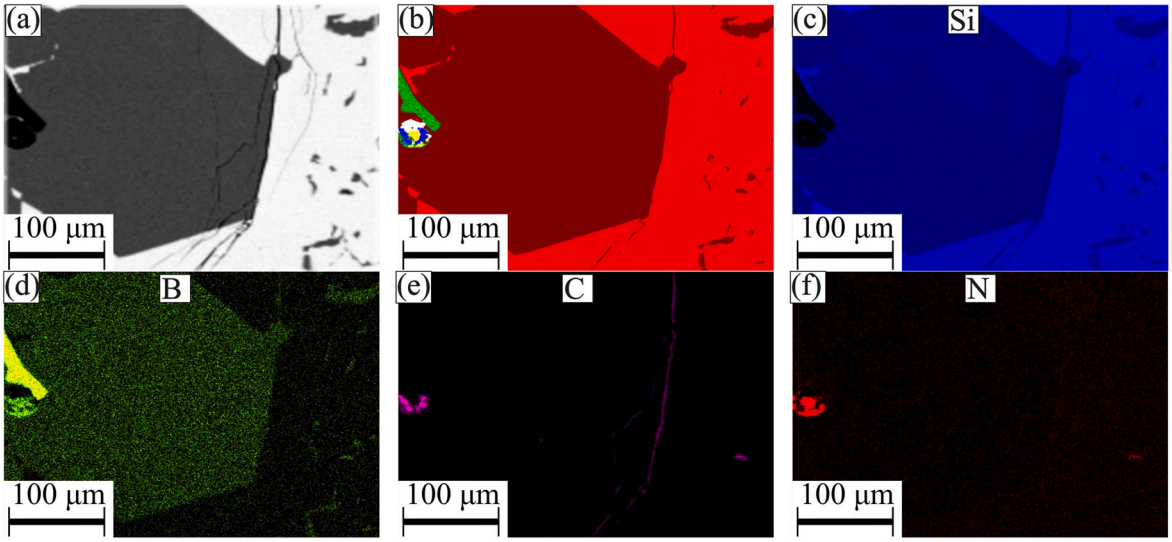

Fig. 4. SEM micrographs and EDS maps of the Si–8B alloy in the Si_3N_4 crucible at 1750 °C. (a) was captured by a secondary electron detector; (b) phase distribution; (c–e) were EDS elemental maps of silicon, boron, carbon, and nitrogen, respectively.

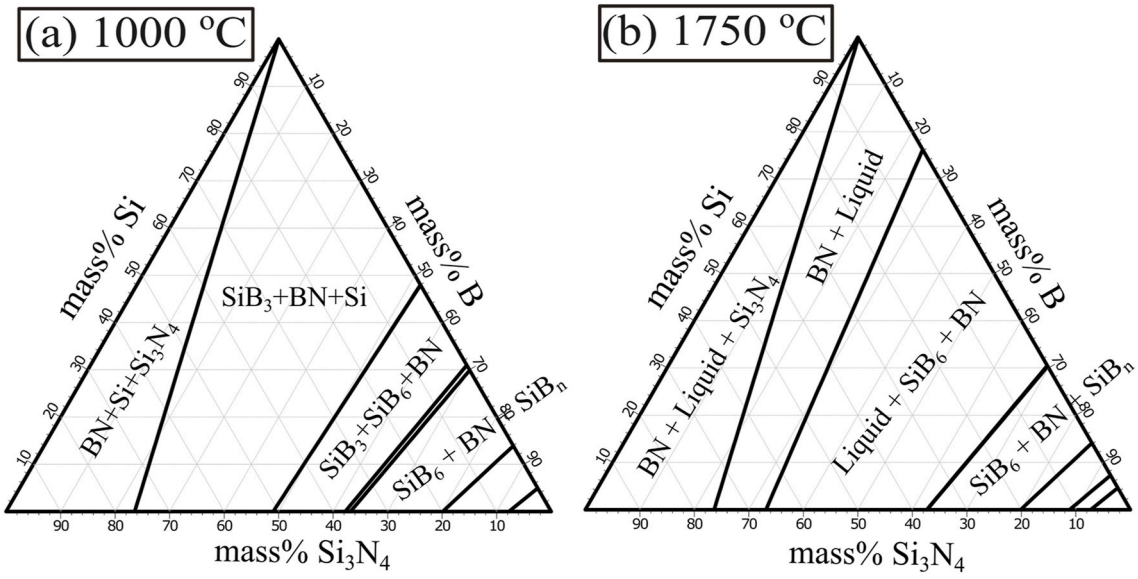

Fig. 5. Calculated isothermal sections in the Si–B– Si_3N_4 system. (a) 1000 °C; (b) 1750 °C. Calculated using the commercial FTlite database [3].

temperature range of 1350–1400 °C. Next, a holding time of 10 min was kept at 1400 °C before natural cooling.

The microstructures were studied by Zeiss Supra, 55 VP Scanning Electron Microscope (SEM) with the feature of Backscattered Electron image (BSE), Energy Dispersive Spectroscopy (EDS), and X-ray element mapping. Moreover, an electron probe micro-analyzer (EPMA) JEOL JXA 8500 was used to generate the elemental mapping. Quantitative measurement of the chemical composition of the formed phases was carried out via wavelength dispersive X-ray spectroscopy (WDS). FactSage software [16] was used in our research to predict thermodynamic properties. FTlite and SINTEF [17] databases were chosen to be used in the calculation process.

3. Results and discussion

3.1. Phase formation in the Si–B alloys

SiB_3, SiB_6, eutectic structure (Si + SiB_3), BN, and Si were formed in the Si–B alloys. Fig. 2a–d shows the microstructures of the Si–B alloys after experiments, with the B addition of 2, 5, 8, and 11 mass %. The formed phases were confirmed by EDS analyses, where each phase was taken in 5 different sites in their areas. The average composition of the detected phases is given in Table 1. It is seen that SiB_3, eutectic structure (Si + SiB_3), and Si were observed in all the Si–B alloys. The amount of SiB_3 phase increased with the increase of B content. Moreover, SiC and B_4C were also detected in the Si–B alloys due to carbon pollution. BN was not easily observed in a low magnification state, as shown in Fig. 2. To further confirm if the BN precipitates produced in the Si–B alloys, the phases formed in the Si–8B alloy were studied in a high magnification state. As shown in Fig. 3b, BN and B_4C are not easily separated in low magnification. It can however be distinguished in a high contrast state, as shown in Fig. 3c. It is seen that the BN precipitates were embedded in the SiB_6 phase. Moreover, the elemental distributions of Si, B, C, and N were carried out in the Si–8B alloy. It is seen from Fig. 4a that three areas were identified based on phase morphology and contrast. It is easy to confirm that the bright region was Si(ss) and the grey particles were SiB_3. However, the dark phase was complex. It is seen from Fig. 4c–e that C and N were accumulated on the bottom side of the dark grains, which consisted of B_4C and BN phases. The top side of the dark grains looked like the pure B phase. However, the measured chemical composition was 82.9 at. % B and 14.2 at. % C in this area. The ratio of B/C was 5.8, which is in the range of 4.3–12 for the B_4C phase [18]. Hence, the dark grain

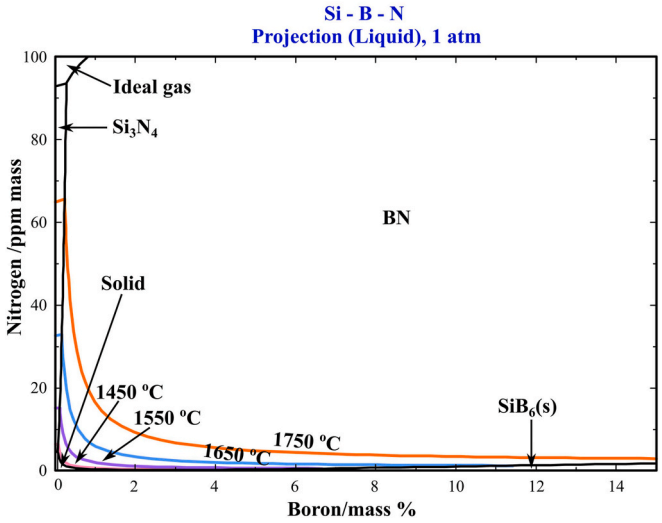

Fig. 6. Liquidus projection of Si–B–N phase diagram. Calculated using the commercial SINTEF database [17].

was believed to be B_4C. BN was formed due to the dissolution of N from the Si_3N_4 crucible, and it was further confirmed by EDS examination with the composition of 53.2 at. % B and 45.4 at. % N in this area.

Fig. 5 shows the isothermal sections of the Si–B–Si_3N_4 system at 1000 °C and 1750 °C, respectively. The calculated phase diagrams show that no stable ternary phase is expected to form in the Si–B–Si_3N_4 system. It is consistent with the data provided by Seifert et al. [19]. It is seen from the isothermal section at 1750 °C (Fig. 5b) that 2–11 mass % B alloys were in the BN + Liquid area. During cooling, the alloys were transferred to the SiB_3 + Si + BN area at 1000 °C (Fig. 5a). The calculated results are in good agreement with our experimental results, regardless of the C pollution.

SiC and B_4C were detected in the Si–B alloys, which was not expected. In the experiments, the charged Si_3N_4 crucibles were placed at the bottom of the graphite crucible (G-2) under Ar flow. The presence of SiC and B_4C may hence be caused by the pollution from the graphite holder.

BN was found in the Si–B alloys (Fig. 3) due to the dissolved N into the liquid Si–B alloys. The formation of BN was caused by the reaction,

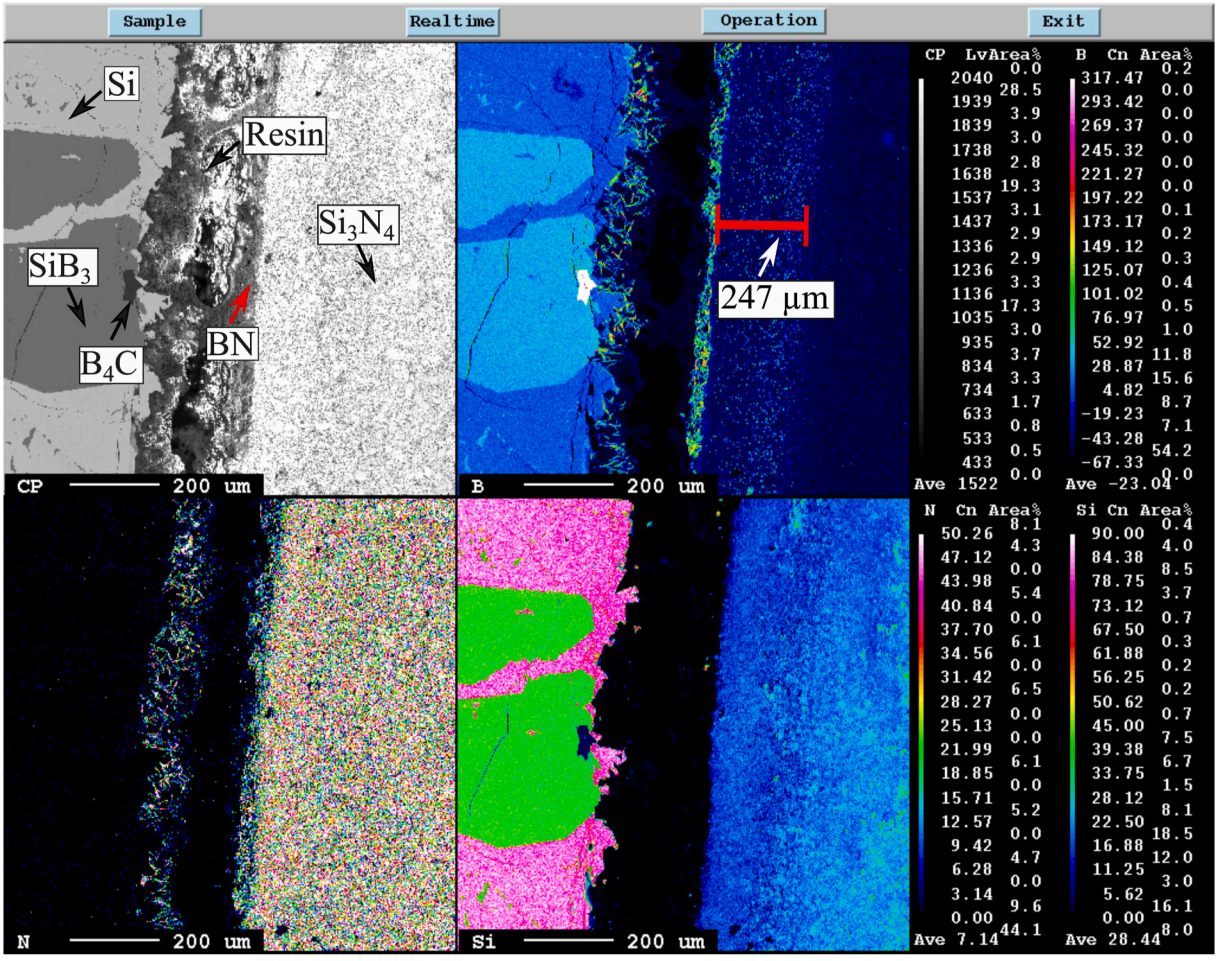

Fig. 7. EPMA elemental map at the interface between the Si–8B alloy and Si_3N_4 crucible at low magnification.

N + B(l) → BN(s). Therefore, the dissolved N results in the formation of BN in Si–B alloys. The N solubility in liquid Si–B alloys was estimated by using the FactSage software package, as shown in Fig. 6. The N solubility is lower than 10 ppm mass at 1750 °C in the liquid Si–B alloys with the 2–11 mass % B addition. Hence, the B content (57.0 at. %) was higher than N (39.7 at. %) in the BN phase (Table 1). The driving force for producing BN is limit, and the amount of BN is limited in the Si–B alloys bulk phase.

3.2. *Interface phase formation between Si–B alloys and Si_3N_4 crucible*

A continuous BN layer was formed at the interface between the Si–B alloys and Si_3N_4 crucible. Fig. 7 and Fig. 8 present the elemental distribution at the interface between the Si–8B alloy and Si_3N_4 in both low and high magnification states, respectively. For the B distribution mapping area, it is seen that the B content was higher in the Si_3N_4 area close to the interface. The phase formed at the interface was further confirmed by WDS analyses with an average composition of 5.6 at. % Si, 30.3 at. % B, and 64.1 at. % N. It indicates that a continuous BN layer was produced at the interface. The B elemental distribution shows that the liquid B would diffuse to the Si_3N_4 crucible and the diffusion depth was measured to be 247 μm. For the N, the results show that the N content was almost negligible in the Si–8B alloy.

There will be some interaction between the Si_3N_4 and the liquid Si–B alloys to form the BN layer. Hence, B in the liquid phase reacts with Si_3N_4 at 1750 °C. On the other hand, the formation of the BN layer might also be caused by the dissolved N, due to the reaction N + B(l) = BN(s). Since the BN is at the Si_3N_4 surface, it is believed that the reaction will happen between the dissolved B and Si_3N_4.

Fig. 9 shows the calculated interaction between the Si–B alloys and Si_3N_4 at 1750 °C. The X-axis represents the content of the Si–B alloys, in which X = 0 shows the Si_3N_4 position and X = 1 shows the Si–B alloys position. The Y-axis represents the mass percent of the formed phase. As it is expected, the formation of BN is possible from the reaction of Si–B alloy and Si_3N_4 at 1750 °C. The amount of BN increases with the increase of B content in the Si–B alloys.

The formation of BN at the Si/Si_3N_4 interface is resulting from the following reaction.

$$B + ¼\ Si_3N_4\ (s) = BN\ (s) + ¾\ Si\ (l) \quad (1)$$

The Gibbs energy, ΔG, of the formation of BN is given as

$$\Delta G = \Delta G^0 + RT \ln (a_{Si}^{¾} \cdot a_{BN})/(a_B \cdot a_{Si3N4}^{¼}) \quad (2)$$

Where R is the gas constant. T is the absolute temperature. a_{BN} and a_{Si3N4} are the activities of BN and Si_3N_4 at solid state, which is assumed to be unity. a_{Si} and a_B are the activities of Si and B at liquid state. ΔG^0 is the standard Gibbs energy of the formation of BN. The calculation results are shown in Fig. 10.

As shown in Fig. 10, the Gibbs energy shows a negative value in the B range 2–11 mass % at 1750 °C, and it decreases with the increase of B content in the Si–B alloys. The negative Gibbs energy indicates that the formation of BN is possible. The developing of the layer of BN at the interface can be explained.

The formation of the BN layer can play the role of barrier coating between the Si–B alloys and the Si_3N_4 crucible. It shows that Si_3N_4 is a potential refractory material as the PCM container in the thermal energy

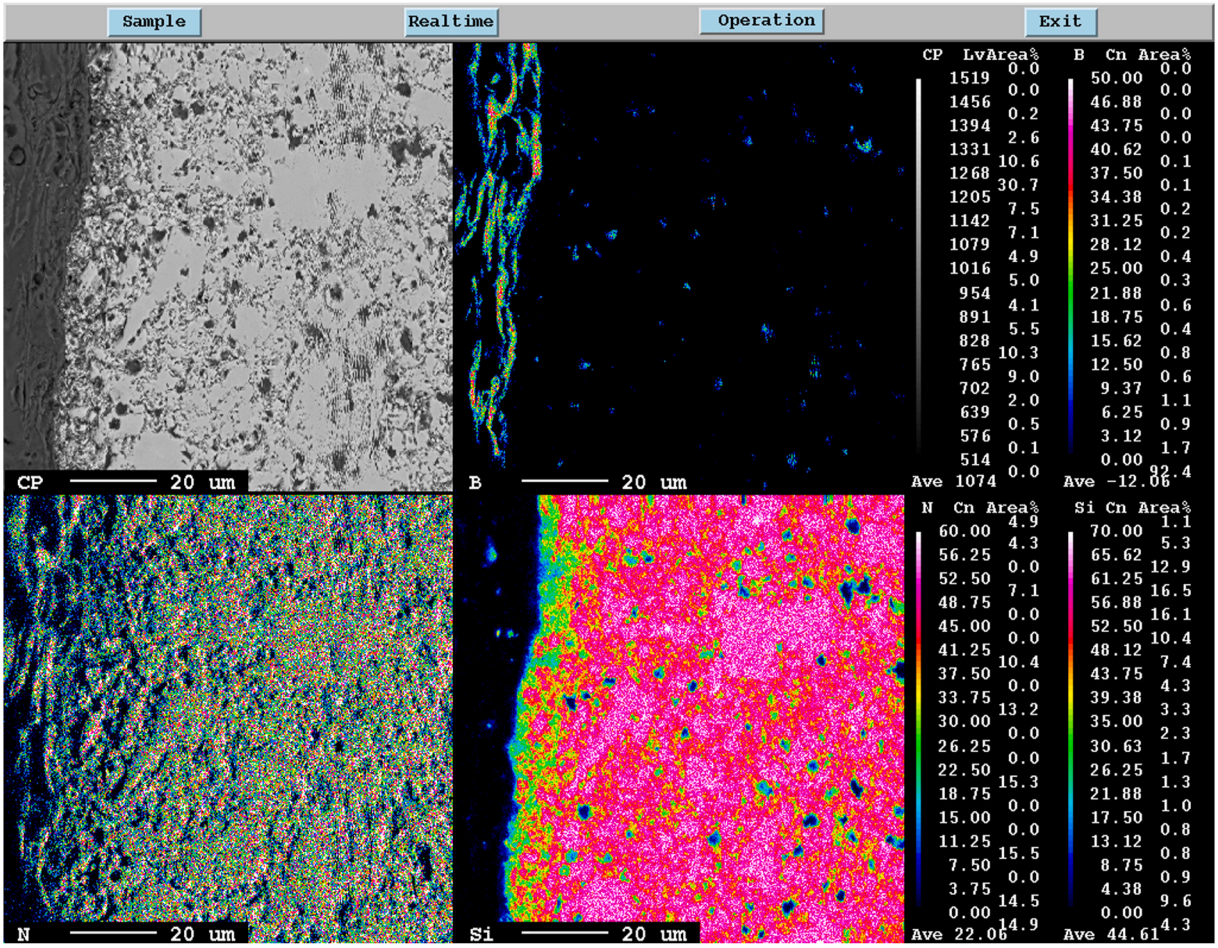

Fig. 8. EPMA elemental map at the interface between the Si–8B alloy and Si_3N_4 crucible at high magnification.

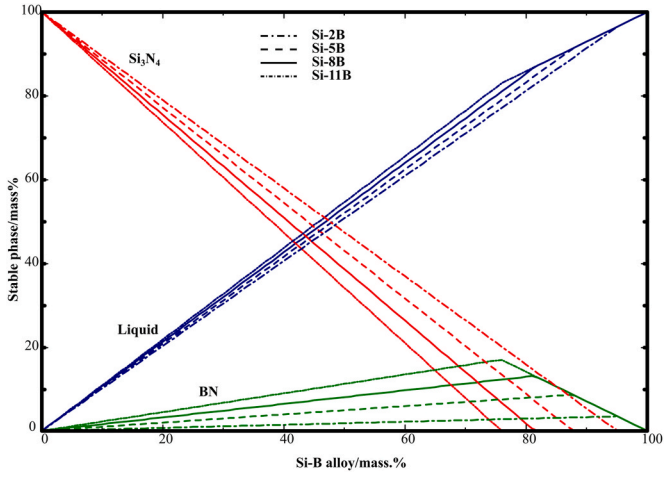

Fig. 9. The interaction between Si_3N_4 crucible and Si–B alloys (2–11 mass % of boron) at 1750 °C. Calculated using the commercial FTlite database [3].

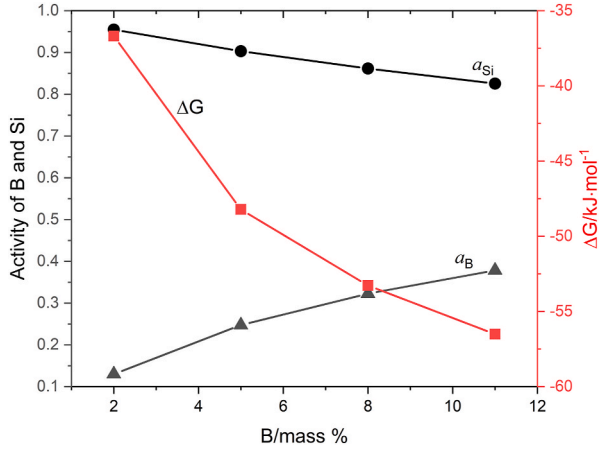

Fig. 10. The function of Gibbs energy and activity with B content at 1750 °C. Calculated using the commercial FTlite database [3].

storage system.

3.3. Wettability behavior of Si-3.25B alloy on Si_3N_4 substrate

The equilibrium contact angle of the liquid Si-3.25B alloy on the Si_3N_4 substrate was measured to be 134 ± 1°. Fig. 11 describes the changing shape of the Si-3.25B particle during the melting/solidification process under 10^{-4} atm. At 1389 °C, the sample started to melt and was completely melted at 1400 °C. The onset temperature was close to the theoretical melting point of 1385 °C [2]. The recorded images show that the solidification started at 1318 °C and finished at around 1200 °C. The contact angles of the Si-3.25B droplet as a function of time are presented in Fig. 12, where the time of zero corresponds to the complete melting at 1400 °C. It is apparent from the figure that the initial contact angle was equal to 134 ± 1° and it was almost constant within the holding time of

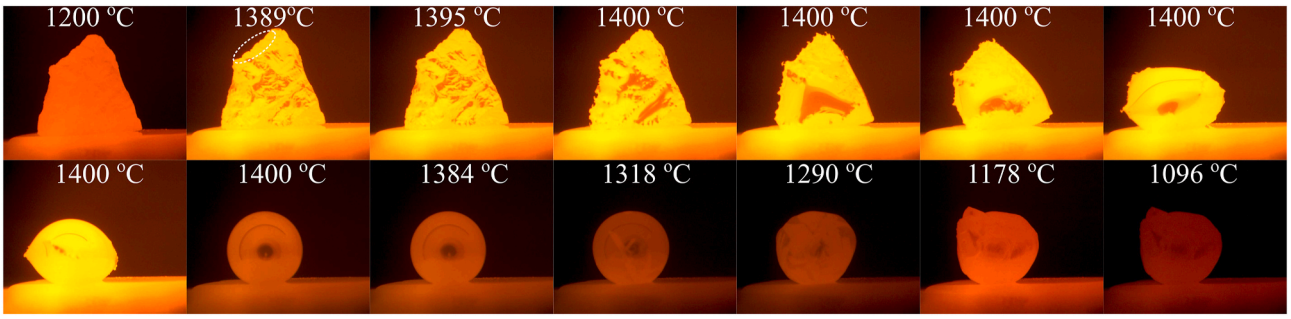

Fig. 11. Wetting test of Si-3.25B alloy on Si_3N_4 substrate under 10^{-4} atm. The white dotted circle represents the volume expansion of Si-3.25B alloy during solidification.

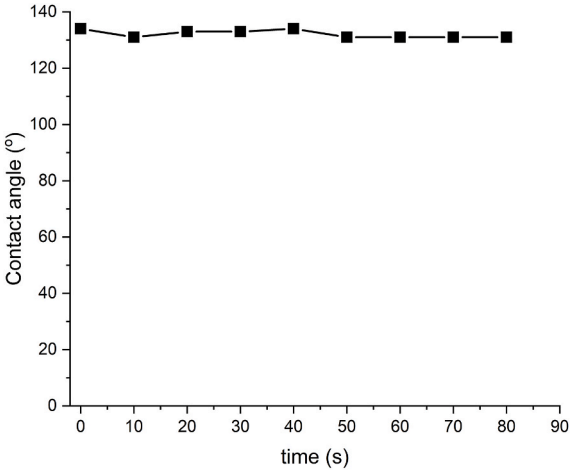

Fig. 12. Contact angle as a function of time for a liquid Si-3.25B drop on Si_3N_4 substrate at 1400 °C.

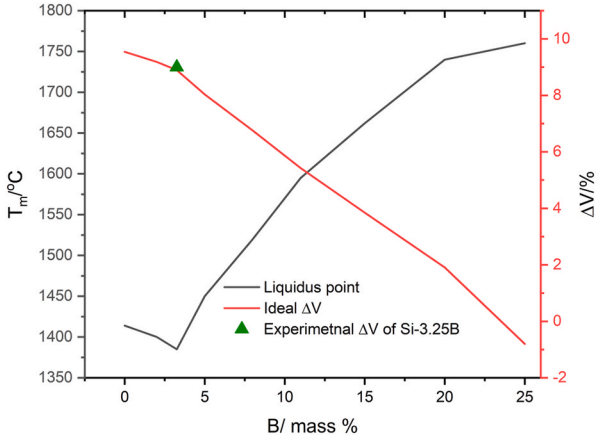

Fig. 13. The volume expansion and the liquidus temperature of the Si–B melts as a function with B content.

80 s.

The value of the contact angle in the Si-3.25B/Si_3N_4 system is higher than that measured in the Si/Si_3N_4 systems (0–90°) in the literature [20–23]. According to Li et al. [20], at the surface of the Si_3N_4 substrate, a thin layer of oxynitride (SiN_xO_y) was formed. Therefore, in the Si/Si_3N_4 system, the initial angle of 85° was contributed to the SiN_xO_y layer. Then, the contact angle was decreased with time and tended to 49°, close to the contact angle between the liquid Si and Si_3N_4. However, in the Si-3.25B/Si_3N_4 system in this work, the contact angle was measured to be 134 ± 1°, close to the wetting angle in the Si/BN system (90–145°) [23–27] and in the Si-3.2B/BN system (144–151°) [28]. Hence, it is believed that a BN layer was formed between the Si-3.25B alloy and Si_3N_4, which is consistent with the experimental results obtained in the Si_3N_4 crucible.

The volume expansion was readily observed in the cooling process, by the final liquid flowing out at the left top of the solidified drop. It shows that the maximum volume change was about 9% from the liquidus point to the complete solidification.

The ideal volume change of Si–B alloys during solidification from the liquidus point to room temperature was calculated based on the density of the formed phases. It should be noted that the solid volume is the sum of Si(*s*) and SiB_6 phases and the solid Si has no B dissolved, while the liquid volume is the sum of Si(*l*) and B(*l*) phases with the assumption of an ideal solution. It is assumed that *a* mole B is mixed with *b* mole Si. Hence, the ideal volume expansion can be expressed as follows:

$$n_{Si(l)} = b,\ n_{B(l)} = a,\ n_{SiB6} = a/6,\ n_{Si(s)} = b\text{-}a/6 \quad (3)$$

Where $n_{Si(l)}$, $n_{B(l)}$, n_{SiB6}, and $n_{Si(s)}$ are the mole of the Si(*l*), B(*l*), SiB_6, and Si(*s*) in the Si–B alloys, respectively. Hence, the volume of the solidified Si–B alloys at 1270 °C (V_s) and the volume of the liquid Si–B alloys (V_l) can be expressed:

$$V_s = (n_{SiB3}\cdot M_{SiB3}/\rho_{SiB3}) + (n_{Si(s)}\cdot M_{Si(s)}/\rho_{Si(s)}) \quad (4)$$

$$V_l = (n_{Si(l)}\cdot M_{Si(l)}/\rho_{Si(l)}) + (n_{B(l)}\cdot M_{B(l)}/\rho_{B(l)}) \quad (5)$$

In the end, the volume change ΔV is expressed as follows.

$$\Delta V = (V_s - V_l)/V_s \cdot 100\% \quad (6)$$

The ideal volume change of a Si–B alloy is calculated based on the above equations. The results are presented in Fig. 13. There are two Y-axis in the figure, in which the left one represents the value of the liquidus temperature, and the right represents the volume change. The X-axis represents the B addition in the Si–B alloys. The green triangle represents the experimental result obtained from the wetting test. It is seen that the volume expansion of Si–B alloys decreases with the increase of B content. It might be caused by the contraction of the Si lattice in an alloy with B [2]. The measured volume change of the Si-3.25B alloy has a good agreement with the calculated result.

4. Conclusions

The present work summarizes the study concerning the use of Si_3N_4 as the Si–B alloys container in the thermal energy storage system. Si, Si + SiB_3 (eutectic structure), SiB_3, SiB_6 are formed in the Si–B alloys. BN precipitates are also recognized after solidification, while the amount of BN is negligible. A continuous BN layer is produced at the interlayer between the Si–B alloys and Si_3N_4 crucible. It can be a barrier layer to prevent the penetration of liquid Si–B alloys to Si_3N_4. In the wetting test, the equilibrium contact angle is measured to be 134 ± 1° between the Si-

3.25B alloy and the Si_3N_4 substrate, which shows non-wetting behavior. Moreover, the volume change in Si-3.25B alloy is measured to be ~ 9%. It still has a high-volume expansion during solidification. All the results show that Si_3N_4 is a suitable refractory material for building Si–B alloys container in the thermal energy storage system.

Declaration of competing interest

The authors declare that they have no known competing financial interests or personal relationships that could have appeared to influence the work reported in this paper.

Acknowledgment

The author acknowledge the fund provided through the Amadeus project (737054) by the European Union's Horizon 2020, and the KPN project controlled tapping (267621) by the Norwegian Research Council together with the Norwegian Ferroalloy-producers Research organization.

References

[1] A. Datas, A. Ramos, A. Martí, C. del Cañizo, A. Luque, Ultra high temperature latent heat energy storage and thermophotovoltaic energy conversion, Energy 107 (2016) 542–549, https://doi.org/10.1016/j.energy.2016.04.048.
[2] R.W. Olesinski, G.J. Abbaschian, The B-Si (Boron-Silicon) system, Bull. Alloy Phase Diagrams 5 (1984) 478–484, https://doi.org/10.1007/BF02872900.
[3] M.R. Gilpin, High Temperature Latent Heat Thermal Energy Storage to Augment Solar Thermal Propulsion for Microsatellites, 2015.
[4] J. Jiao, J. Safarian, B. Grorud, M. Tangstad, High Temperature Interaction of Si-B Alloys with Graphite Crucible in Thermal Energy Storage Systems, 2020, https://doi.org/10.3390/ma13010029.
[5] W. Polkowski, N. Sobczak, A. Polkowska, G. Bruzda, A. Kudyba, D. Giuranno, Silicon as a phase change material: performance of h-BN ceramic during multi-cycle melting/solidification of silicon, JOM 71 (2019) 1492–1498, https://doi.org/10.1007/s11837-019-03364-4.
[6] W. Polkowski, N. Sobczak, G. Bruzda, R. Nowak, D. Giuranno, A. Kudyba, A. Polkowska, K. Pajor, T. Kozieł, I. Kaban, The effect of boron content on wetting kinetics in Si-B alloy/h-BN system, J. Mater. Eng. Perform. (2018) 1–7, https://doi.org/10.1007/s11665-018-3786-8.
[7] J.M. Jiao, Si-based Phase Change Materials in Thermal Energy Storage Systems, Ph. D thesis, NTNU, 2020.
[8] A.K. Søiland, E.J. Øvrelid, O. Lohne, J.K. Tuset, T.A. Engh, Ø. Gjerstad, Carbon and nitrogen contents and inclusion formation during crystallization of multi-crystalline silicon, Proc. 19th EUPVSEC (2004) 7–11.
[9] M. Tanahashit, F. Fujisawa, C. Yamauchi, Activity of boron in molten silicon, Shigen-to-Sozai. 114 (1998) 807–812, https://doi.org/10.2473/shigentosozai.114.807.
[10] M. Takeuchi1, Y. Iguchi, T. Narushima, Nitrogen solubility in liquid silicon, Mater. Trans., JIM 35 (1994) 821–826, https://doi.org/10.2320/matertrans1989.35.821.
[11] T. Yoshikawa, K. Morita, Thermodynamic property of B in molten Si and phase relations in the Si-Al-B system, Mater. Trans. 46 (2005) 1335–1340, https://doi.org/10.2320/matertrans.46.1335.
[12] Y. Yatsurugi, N. Akiyama, Y. Endo, T. Nozaki, Concentration, solubility, and equilibrium distribution coefficients of nitrogen and oxygen in semiconductor silicon, J. Electrochem. Soc. 120 (1973) 975–978, https://doi.org/10.1149/1.2403610.
[13] W. Kaiser, C.D. Thurmond, Nitrogen in silicon, J. Appl. Phys. 30 (1959) 427–431, https://doi.org/10.1063/1.1735180.
[14] H. Du, Thermodynamics of the Si-N-O system and kinetic modeling of oxidation of Si3N4, J. Electrochem. Soc. 136 (1989) 3210, https://doi.org/10.1149/1.2096427.
[15] S. Binetti, M. Acciarri, C. Savigni, A. Brianza, S. Pizzini, A. Musinu, Effect of nitrogen contamination by crucible encapsulation on polycrystalline silicon material quality, Mater. Sci. Eng. B. 36 (1996) 68–72, https://doi.org/10.1016/0921-5107(95)01268-0.
[16] FactSage, (n.d.). http://www.factsage.com/fs_general.php.
[17] K. Tang, E.J. Øvrelid, G. Tranell, M. Tangstad, Thermochemical and kinetic databases for the solar cell silicon materials, Proc. 12th Int. Ferroalloys Congr. Sustain. Futur. (2010) 619–629, https://doi.org/10.1007/978-3-642-02044-5_13.
[18] P. Franke, D. Neuschütz, H. Landolt, R. Börnstein, Binary Systems. Part 2: Elements and Binary Systems from B – C to Cr – Zr, Springer Berlin Heidelberg, Berlin/Heidelberg, 2004, https://doi.org/10.1007/b76783.
[19] S.H. Jürgen, F. Aldinger, Phase Equilibria in the Si-B-C-N System, in: High Perform. Non-oxide Ceram. I, Springer, Berlin/Heidelberg, 2002, pp. 1–58.
[20] J.G. Li, H. Hausner, Influence of oxygen partial pressure on the wetting behaviour of silicon nitride by molten silicon, J. Eur. Ceram. Soc. 9 (1992) 101–105, https://doi.org/10.1016/0955-2219(92)90051-E.
[21] Z. Yuan, W.L. Huang, K. Mukai, Wettability and reactivity of molten silicon with various substrates, Appl. Phys. Mater. Sci. Process 78 (2004) 617–622, https://doi.org/10.1007/s00339-002-2001-8.
[22] B. Drevet, N. Eustathopoulos, Wetting of ceramics by molten silicon and silicon alloys: a review, J. Mater. Sci. 47 (2012) 8247–8260, https://doi.org/10.1007/s10853-012-6663-0.
[23] B. Drevet, R. Voytovych, R. Israel, N. Eustathopoulos, Wetting and adhesion of Si on Si3N4 and BN substrates, J. Eur. Ceram. Soc. 29 (2009) 2363–2367, https://doi.org/10.1016/j.jeurceramsoc.2009.01.024.
[24] Y. Maeda, T. Yokoyama, I. Hide, T. Matsuyama, K. Sawaya, Releasing material for the growth of shaped silicon crystals, J. Electrochem. Soc. 133 (1986) 440–443, https://doi.org/10.1149/1.2108594.
[25] J.A. Champion, B.J. Keene, S. Allen, Wetting of refractory materials by molten metallides, J. Mater. Sci. 8 (1973) 423–426, https://doi.org/10.1007/BF00550164.
[26] J.V. Naidich, The Wettability of Solids by Liquid Metals, Elsevier, 2013, pp. 353–484, https://doi.org/10.1016/b978-0-12-571814-1.50011-7.
[27] W. Polkowski, N. Sobczak, R. Nowak, A. Kudyba, G. Bruzda, A. Polkowska, M. Homa, P. Turalska, M. Tangstad, J. Safarian, E. Moosavi-Khoonsari, A. Datas, Wetting behavior and reactivity of molten silicon with h-BN substrate at ultrahigh temperatures up to 1750 °C, J. Mater. Eng. Perform. (2017) 1–14, https://doi.org/10.1007/s11665-017-3114-8.
[28] W. Polkowski, N. Sobczak, M. Tangstad, J. Safarian, Silicon and silicon-boron alloys as phase change materials in thermal energy storage units, Silicon Chem. Sol. Ind. XIVSilicon Chem. Sol. Ind. XIV. (2018), https://doi.org/10.5281/zenodo.1289792.